Modification of Biodegradable Polylactide by Silica and Wood Flour Through a Sol–Gel Process

Chin-San Wu, Hsin-Tzu Liao

Department of Chemical and Biochemical Engineering, Kao Yuan University, Kaohsiung County, Taiwan 82151, Republic of China

Received 27 July 2007; accepted 26 December 2007
DOI 10.1002/app.27988
Published online 2 May 2008 in Wiley InterScience (www.interscience.wiley.com).

ABSTRACT: The aim of this work is the production of new biodegradable nanocomposites from polylactide (PLA), tetraethoxysilane (TEOS), and wood flour (WF) by means of an *in-situ* sol–gel process and a melt blending method. Characterizations of SiO_2, PLA, and hybrids were performed by FTIR, ^{29}Si solid-state NMR, XRD, DSC, TGA, and SEM analyses. As the results, the SiO_2 can be well dispersed into the acrylic acid grafted polylactide (PLA-*g*-AA) in nanoscale sizes since the TEOS is partially compatible with PLA-*g*-AA and allows PLA-*g*-AA chains intercalating into SiO_2 layers. ^{29}Si solid-state NMR analysis showed that Si atoms coordinated around SiO_4 units were predominantly Q_3 and Q_4. The PLA-*g*-AA/SiO_2 hybrid demonstrates dramatic enhancement in thermal and mechanical properties of PLA; for example, 80°C and 20 MPa increases in IDT and TS with the addition of 10 wt % SiO_2 due to the formation of Si—O—C bond, and the nanoscale dispersion of silicate layers in the polymer matrix. On the basis of the consideration of thermal and mechanical properties, it is also found that 10 wt % of SiO_2 content is optimal for preparation of PLA-*g*-AA/SiO_2 nanocomposites. The biodegradable nanocomposites produced from our laboratory can provide a plateau tensile strength at break when the WF content is up to 50 wt %. © 2008 Wiley Periodicals, Inc. J Appl Polym Sci 109: 2128–2138, 2008

Key words: polylactide; SiO_2; blends; sol–gel; wood flour

INTRODUCTION

The nonrenewable of most plastics has caused many environmental problems associated with their disposal. Recycling is an environmentally attractive solution but only a minor portion of plastics is recyclable and most end up in municipal burial sites, thereby leading the increasingly difficult problem of finding available landfill areas. Hence, there is an increased interest in production and use of biodegradable polymers. The main strategies to address these problems are utilization of polymeric materials from renewable sources [e.g. wood flour (WF), starch, cellulose, and chitin] and development of biodegradable polymeric materials [e.g. polylactide (PLA), poly(3-caprolactone) (PCL), poly(glycolic acid) (PGA), and poly(3-hydroxybutyrate) (PHB)].[1–5]

In the past decades, blending of plastic materials with low cost and natural biopolymers to increase the biodegradability of original polymers has received a considerable industrial and academic interest.[6–11] This is due to the advantage that these biopolymers are abundant, inexpensive, renewable, and fully biodegradable natural raw materials. It is now possible to prepare polymer/ceramic hybrids via molecular-level manipulation using a sol–gel process to create novel materials.[12–20] The promise of these new hybrid materials is a controllable combination of benefits of polymers (e.g. flexibility, toughness, and easy processing) and ceramics (e.g. hardness, durability, and thermal stability). Examples of organic polymers used in the sol–gel process include elastomers, glassy polymers, and semicrystalline polymers.[21] Ceramic precursors usually involve organometallic compounds [$M(OC_nH_{2n+1})_z$, where M = Si, Sn, Ti, Zr, Al, etc.], and the most common one is tetraethoxysilane (TEOS).[22,23] Via the sol–gel process, organometallic compounds may be hydrolyzed to liberate terminal hydroxyl groups and then subsequently condense with each other to form metal-oxygen-metal bridging units.

In this study, we attempt to blend PLA with WF and ceramics to lower the cost and to enhance mechanical properties of PLA. The purpose of this article is devoted to prepare biodegradable PLA/SiO_2/WF nanocomposites by the simple melt blending method to mitigate the disadvantages of PLA. It is well known that homogeneous dispersion of the hydrophilic SiO_2 in the hydrophobic PLA matrix does not occur because there is no polar group in the backbone of biopolymer. Therefore, the acrylic acid grafted PLA

Correspondence to: C.-S. Wu (cws1222@cc.kyu.edu.tw).
Contract grant sponsor: National Science Council of the Republic of China; contract grant number: NSC-95-2221-E-244-014-.

(PLA-*g*-AA) was studied as an alternative to PLA. We predict that the PLA-*g*-AA/SiO_2/WF hybrid could obviously improve properties of the PLA/SiO_2/WF hybrid since hydrogen bonds may arise from the basic group of the hydrogen acceptor in the PLA-*g*-AA and the covalent bonds may result from dehydration of —OH groups in the polymer and the residual silica bonded in the silica network. The conclusions are based on a combination of fourier transform infrared (FTIR) spectrophotometer, ^{29}Si solid-state nuclear magnetic resonance (NMR) spectrophotometer, scanning electron microscope (SEM), and X-ray diffractometer (XRD). Moreover, the thermal and mechanical properties of hybrids were also examined with differential scanning calorimetry (DSC), thermogravimetry analyzer (TGA), and Instron mechanical tester.

EXPERIMENTAL

Materials

PLA was used as supplied by Cargill-Dow, and is composed of 95% L-lactide and 5% meso-lactide. Acrylic acid (AA), supplied by Aldrich, was purified by extraction from acetone before use. Benzoyl peroxide (BPO), used as an initiator, was purified by dissolution in chloroform and reprecipitation with methanol. WF, supplied by Zell Wildshausen GMBH, was Celluflex. The grain size distribution of WF is 100% finer than 250 μm, 87% finer than 100 μm, and 37% finer than 50 μm. The moisture content and the apparent density of WF are (8 ± 2)% and 0.10–0.12 g/cm^3, respectively. Tetraethoxysilane (TEOS; Aldrich Chemical Co., Milwaukee, WI) was of reagent grade and was used as received. Other reagents were purified by the conventional methods. The PLA-*g*-AA copolymer was constructed in our laboratory as described below.

Samples preparation

PLA-*g*-AA copolymer

Grafting reaction of AA onto molten PLA was performed by using xylene as an interface agent and BPO as an initiator under a nitrogen atmosphere at (85 ± 2)°C. The reaction lasted for 6 h with a rotor speed of 60 rpm. The grafting percentage was determined by a titration method and the result showed that it was about 5.96 wt % when BPO and AA loadings were kept at 0.3 wt % and 10 wt %, respectively. More information about grafting reaction of AA can be referred to our previous work.[24]

Preparation of hybrids from PLA, PLA-*g*-AA, SiO_2, and WF

A mixture, called ''Sol A,'' was prepared by dissolving a stoichiometric amount (shown in Table I) of TEOS, H_2O, and HCl (as the catalyst) in THF and then stirring it at room temperature for 30 min to obtain a homogeneous solution. According to Table I, a predetermined amount of PLA, PLA-*g*-AA, PLA+WF, or PLA-*g*-AA+WF was put into a Brabender ''Plastograph'' 200Nm Mixer W50EHT instrument with a blade type rotor set at 50 rpm, and at a temperature of 190–200°C. When the polymer had melted completely, Sol A was added and the sol–gel process was allowed to proceed for 20 min. Prior to characterization, each sample was dried at 105°C in a vacuum oven for 3 days to remove residual solvents. Hybrid products were pressed into thin plates using a hot press at 190°C and then put into a dryer for cooling, after which they were made into standard specimens for characterization.

TABLE I
Compositions of Various Sol–Gel Liquid Solutions for Preparation of Hybrid Materials

	SiO_2 (wt %)				
Compositions	3	7	10	13	16
Polymer (g)[a]	38.52	34.01	30.77	28.58	26.26
Sol A					
TEOS (g)	4.13	8.81	11.89	14.65	16.96
THF (g)	4.13	8.81	11.89	14.65	16.96
[HCl]/[TEOS][b]	0.01	0.01	0.01	0.01	0.01
[H_2O]/[TEOS][b]	2.2	2.2	2.2	2.2	2.2

[a] Polymer is PLA, PLA-*g*-AA, PLA+WF, or PLA-*g*-AA+WF.
[b] The mole ratio of HCl and H_2O to TEOS.

Characterizations of hybrids

FTIR analysis

Using thin film samples of the hybrid product, grafting of AA onto PLA was investigated using an FTIR spectrophotometer (BIO-RAD FTS-7PC type). The incorporation of the silicate phase into hybrids, to such an extent that Si—O—Si and Si—O—C bonds were formed, was also verified via the FTIR analysis.

^{29}Si solid-state NMR analysis

^{29}Si NMR spectra were recorded on a Bruker MSL-400 NMR spectrometer, using a standard double air bearing cross polarization/magic angle spinning probe, operated at a frequency of 79.5 MHz for ^{29}Si. Samples were loaded into 4-mm fused zirconia tubes and sealed with Kel-F^{TM} caps. Spectra were obtained at a spinning rate of about 4700 Hz, with other conditions as proposed by Young et al.[25] The ^{29}Si solid-state NMR spectrum was used to study the degree of molecular connectivity of the silicate phase.

XRD analysis

Structural changes in the hybrids were investigated by comparison of X-ray diffraction data obtained from PLA, PLA-*g*-AA, and hybrids, recorded with a Rigaku D/max 3V XRD, using Cu-Kα radiation at a scanning rate of 2°/min.

DSC analysis

The glass transition temperatures (T_g) of samples with sizes ranging from 4 to 6 mg were determined using a TA Instrument 2010 DSC system, in which the melting curves were taken between −30 and 250°C, with a heating rate of 10°C/min.

TGA analysis

A TGA (TA Instrument 2010 TGA) was used to assess whether organic–inorganic phase interactions influenced the thermal degradation of hybrids. Samples were placed in alumina crucibles and tested with a thermal ramp over a temperature range of 30–600°C, at a heating rate of 20°C/min, after which their initial decomposition temperature (IDT) was obtained.

SEM analysis

A SEM (Hitachi microscope Model S-1400, Japan) was used to study the morphology of hybrids and to measure the WF phase size in polymers. Before the tests, the hybrid was prepared in a thin film by a hydrolytic press and then the film was treated with hot water in 80°C for 24 h. Afterward, the film was coated with gold and observed by SEM.

Mechanical testing

The Instron mechanical tester (Model LLOYD, LR5K type) was used to measure the tensile strength and the elongation at break according to the ASTM D638 method. The films of testing samples, which were conditioned at (50 ± 5)% relative humidity for 24 h prior to the measurements, were prepared in a hydrolytic press at 190°C and then the measurements were done using a 20 mm/min crosshead speed. Five measurements were performed for each sample and the results were averaged to obtain a mean value.

RESULTS AND DISCUSSION

Infrared and ^{29}Si solid-state NMR spectroscopy

Figure 1(A–D) shows the FTIR spectra of PLA, PLA-*g*-AA, PLA/SiO_2 (10 wt %), and PLA-*g*-AA/SiO_2 (10 wt %), respectively. It can be seen that all characteristic peaks of PLA at 2800–3000 cm^{-1} appear in four polymers.[26,27] The spectrum of PLA-*g*-AA [Fig. 1(B)] also indicates a broad O—H stretching absorbance at about 3000–3600 cm^{-1}, absent in the PLA spectrum [Fig. 1(A)]. Similar results have been reported elsewhere.[24,28] The PLA-*g*-AA/SiO_2 hybrid also produced a broad O—H bond stretching at about 3000–3600 cm^{-1} [Fig. 1(D)]. This is due to the formation of hetero-associated hydrogen bonds between carboxylic acid groups of PLA-*g*-AA and the silica bonded group.[29]

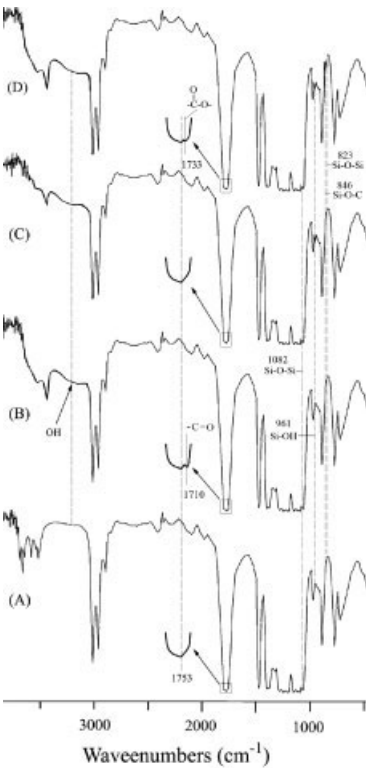

Figure 1 FTIR spectra for (A) pure PLA, (B) PLA-*g*-AA, (C) PLA/SiO_2 (10 wt %), and (D) PLA-*g*-AA/SiO_2 (10 wt %).

New peaks, at about 3000–3600, 1000–1800, 900–1000, and 800–900 cm^{-1}, appeared in the FTIR spectrum of the PLA/SiO_2 (10 wt %) and PLA-*g*-AA/SiO_2 (10 wt %) composite [Fig. 1(C,D)]. The broad peak at about 3000–3600 cm^{-1} in spectra of PLA/SiO_2 and PLA-*g*-AA/SiO_2 is due to the existence of O—H groups (Si—OH) and the formation of hydrogen bonds, while peaks in the range 1200–700 cm^{-1} indicate the SiO_2 phase. Peaks between 800 and 1800 cm^{-1} are the result of Si—O—Si (1082 cm^{-1}) and Si—OH (961 cm^{-1}) bonds. The coordinated bond (Si—O—C, 846 cm^{-1}) between PLA and SiO_2 network is absent. Signature of network-forming in the SiO_2 phase is a peak at around 823 cm^{-1}, representing the symmetric vibration of Si—O—Si groups [$(Si—O—Si)_{sym}$]. Although the symmetric vibration

of Si—O—Si is theoretically FTIR inactive, its presence is attributed to distortion of bonding symmetry about the SiO_4 tetrahedral. The absorbance at 846 cm^{-1} is caused by a Si—O—C group, which may be produced from the reaction between PLA-*g*-AA and the silica bonded.[16] Meanwhile, the Si—OH vibration absorbance (~961 cm^{-1}) is a measure of the number of uncondensed silanol groups. Hence, the relative absorbance of these two types of bands (Si—O—Si and Si—OH) allows an assessment of the degree of crosslinking within incorporated silicon oxide phases. The observed stretching vibration of $(Si—O—Si)_{asym}$ (asymmetric) at 1000–1100 cm^{-1} [Fig. 1(C,D)] represents condensation reactions between Si—OH groups. Noticeably, the $(Si—O—Si)_{asym}$ vibration consists of two components arising from Si—O—Si groups in loops (~1082 cm^{-1}), indicated ''cyclic'' in Figure 1(C,D).[30] Consequently, a cyclic component absorbance magnitude contributes to understanding the degree of molecular connectivity within the silicon oxide phase.

On the basis of above observations, it may be supposed that the interfacial force between PLA matrix and SiO_2 network is facilitated only by hydrogen bonds. Comparing the spectra of PLA-*g*-AA and PLA-*g*-AA/SiO_2 [Fig. 1(B,D)], it is found that there is a peak at 1710 cm^{-1}, assigned to —C=O, in the former. In the latter, the peak at 1710 cm^{-1} was shifted to 1733 cm^{-1} due to the formation of ester groups through the reaction between carboxylic acid groups of PLA-*g*-AA and Si—OH groups of SiO_2 network.[15,31] The absorbance of free Si—OH groups appeared at a region, about 961 cm^{-1} in Figure 1(D) (labeled as isolated or free hydroxyl groups).

To better understand the hydrogen-bonding interaction between PLA-*g*-AA matrix and SiO_2 network, FTIR spectra of PLA-*g*-AA copolymer and PLA-*g*-AA/SiO_2 hybrids with different amounts of SiO_2 were expanded in the limited range of 3000–3600 cm^{-1} (Fig. 2). For the PLA-*g*-AA copolymer [Fig. 2(A)], the hydroxyl-stretching band appears as a strong broad band centered at 3288 cm^{-1}. For PLA-*g*-AA/SiO_2 hybrids [Fig. 2(B–D)], the vibration band broadened with an increment of SiO_2 content and it was shifted to 3243, 3195, and 3156 cm^{-1} for 3, 10, and 16 wt % SiO_2, respectively. Above observations demonstrate the existence of strong hetero-associated hydrogen bonds between carboxylic acid groups of PLA-*g*-AA matrix and Si—OH groups of SiO_2 network. In addition, because H-bonds between —COOH groups are stronger than those between —COOH and Si—OH groups, increasing SiO_2 content shifts the wave number to a lower value (lower stretching energy). As for the peak broadening, this is attributed to the increasing amount of —OH groups with an increase in SiO_2 content.

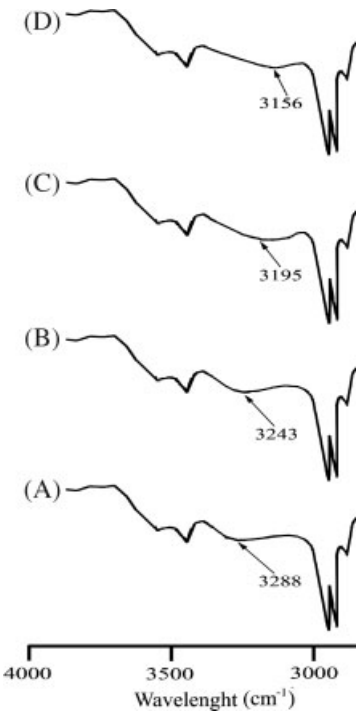

Figure 2 FTIR spectra in the limited range of 3000–3600 cm^{-1} for (A) PLA-*g*-AA, (B) PLA-*g*-AA/SiO_2 (3 wt %), (C) PLA-*g*-AA/SiO_2 (10 wt%), and (D) PLA-*g*-AA/SiO_2 (16 wt%).

^{29}Si solid-state NMR spectra were used to study the degree of molecular connectivity of silicate phase. Peak assignments for different degrees of Si atom substitution about the SiO_4 tetrahedral have been discussed in earlier studies of organic/silica hybrids.[32] Peaks are generally denoted by the symbol Q_n for the Si atom coordination state $(RO)_{4-n}Si(OSi)_n$, where R = H or an alkyl group. Each peak is located within a range of chemical shifts relative to $Si(Me)_4$, as follows: $Q_1 = -68$ to -83 ppm, $Q_2 = -74$ to -93 ppm, $Q_3 = -91$ to -101 ppm, and $Q_4 = -106$ to -120 ppm. Table II and Figure 3 display ^{29}Si solid-state NMR spectra of PLA-*g*-AA/SiO_2 hybrids containing 3, 10, and 16 wt % SiO_2. It can be seen that the chemical shift distribution consists almost exclusively of Q_3 and Q_4 species, with Q_2 species in evidence at higher SiO_2 content. This result implied that the silica has reacted with the PLA-*g*-AA copolymer in hybrids containing lower content of SiO_2. On the other hand, the appearance of Q_2 in the spectrum indicates that silica introduced into the hybrid is in excess. Table II also shows how the Q_2 intensity increases with an increasing of SiO_2 content above 10 wt %. This is because, at content above 10 wt %, silanol groups do not react with PLA-*g*-AA but instead take part in a self-coordination reaction, thus leading to an increase of Q_2. It can also be seen from Figure 3 and Table II that the intensity of Q_3 increases but the intensity of Q_4 slightly decreases

TABLE II
Relative Proportions of Q_n in POE-*g*-AA/SiO_2 Hybrids

SiO_2 (wt %)	Relative proportions (%)		
	Q_2	Q_3	Q_4
3	0	37	63
7	0	41	59
10	0	46	54
13	2	49	49
16	4	52	46

with an increasing of SiO_2 content. This may indicates that Q_4 transformed into Q_3 as the SiO_2 content increased. The relative degree of Q_3 and Q_4 coordination states is in agreement with the structural interpretation of the results and it might be inferred that the degree of porosity is present since ''porous'' silicate nanoparticles have a considerable degree of intramolecular disconnection.[15,33]

To understand the effect of WF content on biodegradable hybrids, the FTIR spectrophotometer was used to examine PLA/WF (30 wt %), PLA-*g*-AA/WF (30 wt %), and PLA-*g*-AA/SiO_2 (7.7 wt %)/WF(30 wt %) and the results are illustrated in Figure 4(A–C), respectively. In Figure 4, all the characteristic peaks of PLA can be seen in the three polymers. It is also found that a broad O—H bond stretching in 3000–3600 cm^{-1} appears in the FTIR spectrum of PLA/WF (30 wt %) blend. For the case of PLA-*g*-AA/WF (30 wt %), Figure 4(B), besides the common peaks appear in the spectrum of PLA/WF (30 wt %) blend, there is a new absorption peak (at about 1738 cm^{-1}) corresponding to the ester carbonyl stretching

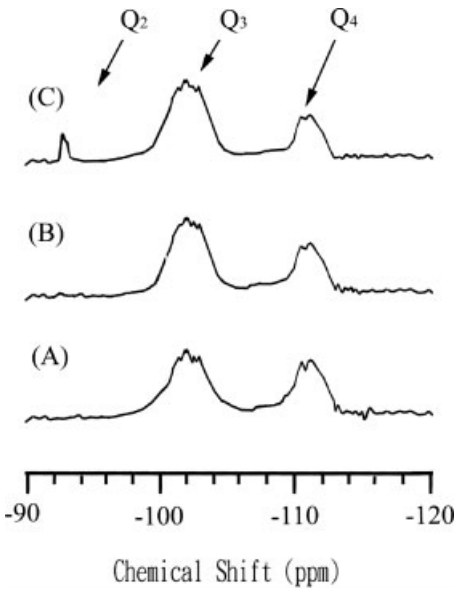

Figure 3 ^{29}Si solid-state NMR spectra of PLA-*g*-AA/SiO_2 hybrids with different silica contents: (A) 3 wt %, (B) 10 wt %, and (C) 16 wt %.

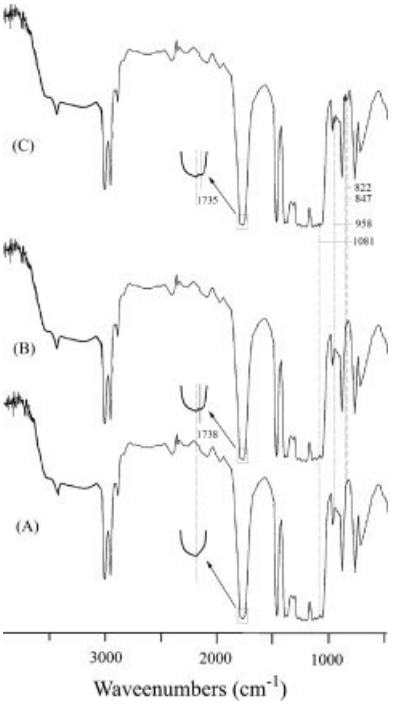

Figure 4 FTIR spectra of (A) PLA/WF (30 wt %), (B) PLA-*g*-AA/WF (30 wt %), (C) PLA-*g*-AA/SiO_2 (7.7 wt %)/WF (30 wt %).

vibration in the copolymer. According to the result proposed by our previous study,[34] there was an absorption peak at 1735 cm^{-1} for the ester carbonyl group. So, the appearance of this new absorption peak at about 1738 cm^{-1} may be due to the formation of an ester carbonyl functional group from the reaction between —OH groups of WF and —COOH groups of PLA-*g*-AA. As the comparison between FTIR spectra of PLA-*g*-AA/WF and PLA-*g*-AA/SiO_2/WF hybrids, Figure 4(B,C), it can be seen that some extra peaks (1100–1000, 950–1000, and 800–850 cm^{-1}) appear in the spectrum of the latter one. As discussed previously, those extra peaks are the consequence due to the characteristic frequencies of SiO_2 and the formation of Si—O—C bond.

Hybrid morphology

To prove the formation of nanocomposites and to study the distribution and the phase size of WF in the polymer matrix, the tensile fracture surface of hybrids was examined by SEM. The SEM microphotographs of PLA, PLA/SiO_2, and PLA-*g*-AA/SiO_2 are presented in Figure 5. From Figure 5(B), it can be seen that the SiO_2 aggregates on the surface of PLA since the silicate can be only dispersed physically in the PLA matrix. Figure 5(C) shows that stacked silicate layers can be exfoliated into nanometer-size layers and uniformly dispersed in the PLA-*g*-AA matrix. SEM microphotographs with magnification

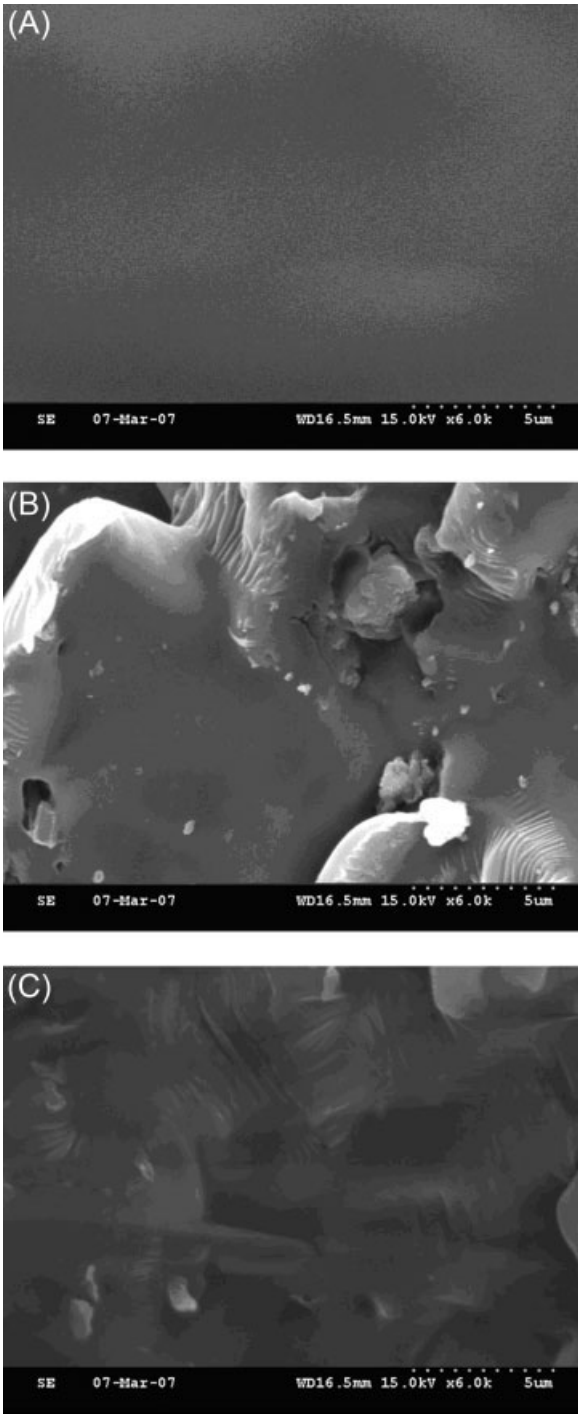

Figure 5 SEM micrographs of (A) pure PLA, (B) PLA/SiO_2 (10 wt %), and (C) PLA-*g*-AA/SiO_2 (10 wt %).

of 600× for PLA/WF (30 wt %) and PLA-*g*-AA/SiO_2 (7.7 wt %)/WF (30 wt %) are shown in Figure 6. Figure 6(A) shows that WF tends to agglomerate into bundles and becomes unevenly distributed throughout the PLA matrix. The bad dispersion of WF in the PLA matrix is due to the wide difference in character between the hydrophobic PLA and the hydrophilic WF. The marker in Figure 6(A) also shows the poor wetting of WF when PLA/WF was used. The reason for this is the large difference in the surface energy between WF and the PLA matrix.[20] For the PLA-*g*-AA/SiO_2 (7.7 wt %)/WF(30 wt %) blend, as shown in Figure 6(B), there is a better dispersion and homogeneity of the WF in the PLA-*g*-AA/SiO_2 matrix. It can also be seen from Figure 6(B) that better wetting is obtained since layers of the matrix material have been pulled out together with the WF, covering the entire WF. The reasons for this result are the more similar character between the WF surface and the PLA-*g*-AA/SiO_2 matrix, and the formation of Si—O—C bonds in the PLA-*g*-AA/SiO_2 hybrid.

With different WF contents, the average pore diameter, i.e. the phase size of WF, of fractured surface of hybrids (PLA/WF, PLA-*g*-AA/WF and PLA-*g*-AA/SiO_2/WF) can be measured from their SEM micrographs (not shown here) and summarized in Table III. It is found that the phase size of WF increases with an increasing content of WF and that the PLA-*g*-AA/SiO_2/WF hybrid has a smaller phase size than other two. For instance, WF phase sizes of

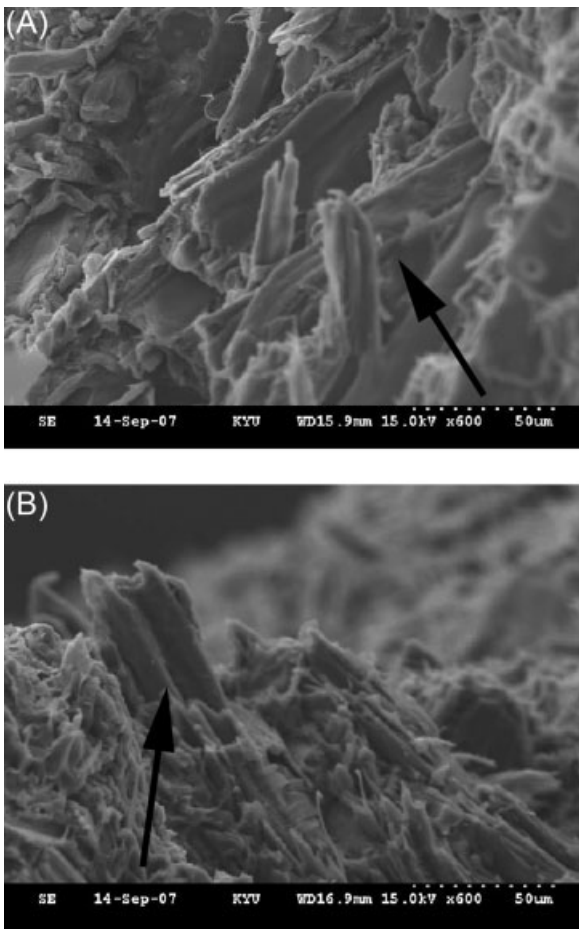

Figure 6 SEM micrographs of (A) PLA/WF (30 wt %) and (B) PLA-*g*-AA/SiO_2 (7.7 wt %)/WF (30 wt %).

TABLE III
The WF Phase Size of PLA/WF, PLA-*g*-AA/WF, and PLA-*g*-AA/SiO_2/WF Hybrids at Different WF Contents

	Phase size (μm)		
WF (wt %)	PLA	PLA-*g*-AA	PLA-*g*-AA/SiO_2 (10 wt %)
10	2.3 ± 0.2	1.3 ± 0.1	0.9 ± 0.1
20	3.0 ± 0.3	1.6 ± 0.2	1.1 ± 0.1
30	3.8 ± 0.4	2.0 ± 0.2	1.3 ± 0.1
40	4.5 ± 0.5	2.3 ± 0.3	1.6 ± 0.2
50	5.1 ± 0.6	2.6 ± 0.3	1.9 ± 0.3

PLA/WF (30 wt %), PLA-*g*-AA/WF (30 wt %) and PLA-*g*-AA/SiO_2 (7.7 wt %)/WF(30 wt %) are 3.8 ± 0.4, 2.0 ± 0.2, and 1.3 ± 0.1 μm, respectively. It is realized that the large phase size of WF produced suggests poor adhesion and compatibility between WF and polymer matrix. So, the PLA-*g*-AA/SiO_2/WF hybrid provided the best dispersion and homogeneity of WF in the polymer matrix.

X-ray diffraction

To further investigate crystalline structures of PLA, PLA/SiO_2, and PLA-*g*-AA/SiO_2, X-ray diffraction patterns at 10–45° (2θ) were examined. Similar to the result obtained by Tsuji et al.,[35] there are two peaks at about 2θ = 16.9° and 2θ = 19.5° in the XRD pattern of unmodified PLA [Fig. 7(A)]. A comparison between XRD patterns of PLA and PLA/SiO_2, Figure 7(A,B), it can be seen that a new peak at 2θ = 40.6° appears in the latter. One can assign the appearance of this new peak to the generation of a silanol functional group in the silica network.[36] As compared with PLA/SiO_2, the XRD pattern of PLA-*g*-AA/SiO_2 [Fig. 7(C)] reveals an extra peak at 2θ = 18.2°. This new peak at 2θ = 18.2°, which may be due to the formation of an ester carbonyl functional group as described in the discussion of FTIR analysis, was also reported by Wu and Liao.[31]

Thermal stability of hybrids (DSC and TGA tests)

Thermal properties of hybrids with various SiO_2 contents were obtained via DSC and TGA tests, and the results are given in Figures 8 and 9. The glass transition temperature (T_g) of hybrid composites is associated with a cooperative motion of long-chain segments, which may be hindered by the SiO_2. Therefore, as expected, PLA-*g*-AA/SiO_2 recorded higher glass transition temperatures than the PLA-*g*-AA copolymer (Fig. 8). It may be suggested that the enhancement in T_g for PLA-*g*-AA/ SiO_2 hybrids is due to the reason that the SiO_2 phase is able to form chemical bonds on hydroxyl groups sites provided by the carboxylic acid groups of PLA-*g*-AA. These strong bonds are able to hinder the motion of the polymer chains. It can be seen that the enhancement on the T_g is not marked for the SiO_2 content beyond 10 wt %. This result might be due to the low-grafting percentage (about 5.96 wt %) of the PLA-*g*-AA copolymer since the increment of T_g is dependent on the number of functional groups in the copolymer matrix to react with the hydroxyl groups in the SiO_2.[37] With SiO_2 content above 10 wt %, they are

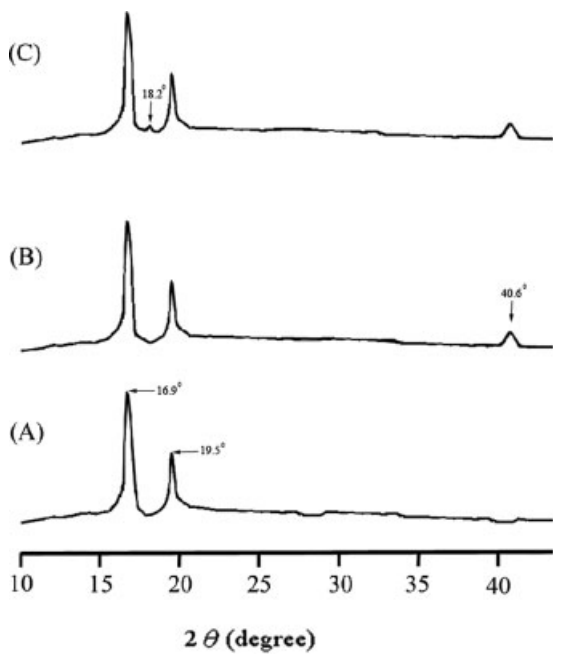

Figure 7 X-ray diffraction patterns for (A) pure PLA, (B) PLA/SiO_2 (10 wt %), and (C) PLA-*g*-AA/SiO_2 (10 wt %).

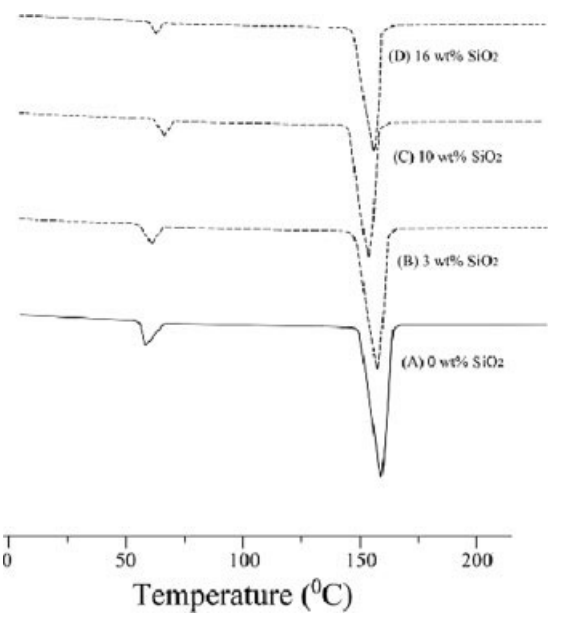

Figure 8 DSC heating thermograms of PLA-*g*-AA and its blends with different amounts of SiO_2.

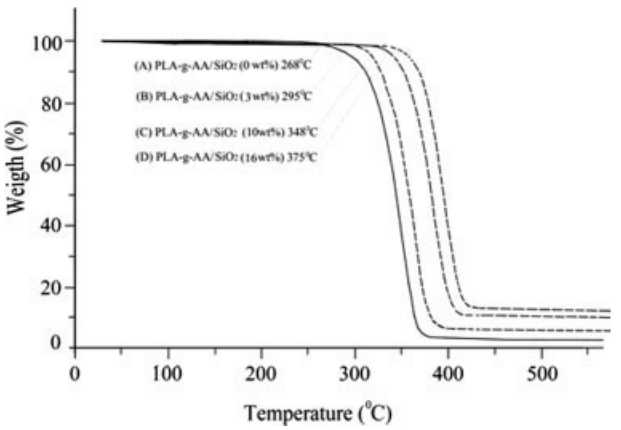

Figure 9 TGA curves for PLA-*g*-AA and its blends with different contents of SiO_2.

dispersed physically in the polymer matrix. Such excess SiO_2 might cause the separation between organic and inorganic phases and lower their compatibility, causing the enhancement on the T_g value became slightly. Figure 8 also shows the melting temperature (T_m) decreases markedly with an increasing of SiO_2 content up to 10 wt % and then the effect is slight. The marked decrease in T_m of PLA-*g*-AA/TiO_2 is probably due to the result of the SiO_2 prohibiting the movement of the polymer segments, causing polymer chain arrangement to become more difficult, and also due to the hydrophilic character of SiO_2 leading to poor adhesion with the hydrophobic PLA.

Table IV summarizes thermal properties (T_g, T_m, IDT, and ΔH_m) of PLA/SiO_2 and PLA-*g*-AA/SiO_2 hybrids. As expected, PLA/SiO_2 and PLA-*g*-AA/SiO_2 hybrids record higher glass transition temperatures than pure PLA. It was also found that the enhancement in T_g for PLA-*g*-AA/SiO_2 hybrids is more significant than that for PLA/SiO_2 hybrids. This is because Si—OH groups are able to form chemical bonds on —COOH sites provided by the carboxylic acid groups of PLA-*g*-AA/SiO_2. These bonds are stronger than the hydrogen bonds in PLA/SiO_2 and therefore are able to hinder the motion of the polymer chains. Table IV also shows how the melt temperature (T_m) decreases with increasing SiO_2 content for PLA/SiO_2, whereas for PLA-*g*-AA/SiO_2, the lowest T_m occurred at 10 wt % SiO_2. Notably, T_m values for all PLA-*g*-AA/SiO_2 hybrids are lower than their PLA/SiO_2 equivalents. This lower melt temperature of PLA-*g*-AA/SiO_2 makes it a more easily processed blend.

Table IV shows that the melt heat (ΔH_m) of pure PLA was 38.2 ± 0.8 J/g. The value of this parameter increases with the crystal formation while it decreases as the SiO_2 content increases. The decrease in crystallization is probably caused by increased difficulty in arranging the polymer chain because of SiO_2 prohibiting movement of the polymer segments. Another potential cause is the hydrophilic character of SiO_2, which would lead to poor adhesion with the hydrophobic PLA. Table IV also shows that ΔH_m decreases with increasing SiO_2 content for PLA/SiO_2 and PLA-*g*-AA/SiO_2 hybrids. Additionally, ΔH_m is about 2–6 J/g higher with PLA-*g*-AA in the composite in place of PLA. Higher ΔH_m is caused by the formation of the ester carbonyl functional group from the reaction between the —OH group of Si—OH and the —COOH group of PLA-*g*-AA.

In the present study, we used thermal gravity analysis (TGA) to determine the effect of SiO_2 content on the weight loss of hybrids, and the result is illustrated in Figure 9. Beside PLA-*g*-AA/SiO_2 hybrids, TGA curves of PLA/SiO_2 hybrids were also made (not shown here) and the detailed IDT values of both hybrids are given in Table IV. It can be seen from Table IV that the IDT value of PLA/SiO_2 and PLA-*g*-AA/SiO_2 hybrids increases with an increasing of SiO_2 content. The increase in IDT is probably caused by the increased difficulty in arranging the polymer chain, due to SiO_2 prohibiting movement of the polymer segments. Another potential cause is the character of SiO_2, which would lead to condensation reaction adhesion with the PLA-*g*-AA. Ji et al.[38] studied the properties of poly(2-hydroxyethyl methacrylate)/SiO_2 blends, reported similar phenomena. For the PLA-*g*-AA/SiO_2 hybrid, the increment of IDT is about 80°C for 10 wt % SiO_2 but the increment is only 27°C as the SiO_2 content is increased

TABLE IV
Thermal Properties of PLA/SiO_2 and PLA-*g*-AA/SiO_2 Hybrids

	PLA/SiO_2				PLA-*g*-AA/SiO_2			
SiO_2 (wt%)	T_g (°C)	T_m (°C)	IDT (°C)	ΔH_m (J/g)	T_g (°C)	T_m (°C)	IDT (°C)	ΔH_m (J/g)
0	57.8	160.5	273	38.2 ± 0.8	56.9	158.6	268	36.8 ± 0.7
3	58.8	159.1	281	33.2 ± 0.7	61.6	156.5	295	35.8 ± 0.7
7	59.7	157.8	298	30.3 ± 0.5	64.2	154.6	320	33.9 ± 0.6
10	61.5	156.3	315	26.1 ± 0.5	68.5	151.7	348	31.3 ± 0.5
13	60.1	157.1	326	24.2 ± 0.4	64.5	153.1	361	28.8 ± 0.5
16	59.3	157.7	338	22.3 ± 0.3	62.2	154.4	375	26.9 ± 0.4

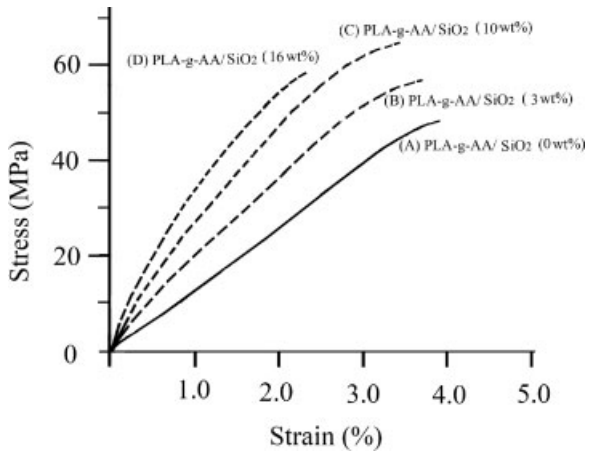

Figure 10 Representative stress–strain curve for PLA-*g*-AA-based composites for a range of SiO_2 content.

from 10 wt % to 16 wt %. This result further confirmed that the optimal loading of SiO_2 is 10 wt % because excess SiO_2 will cause separation of the organic and inorganic phases and lowering their compatibility.

In addition, the residual yields of the PLA-*g*-AA/SiO_2 nanocomposites increased with increasing SiO_2 content, indicating that thermal decomposition of the polymer matrix was retarded in the PLA-*g*-AA/SiO_2 nanocomposites with higher residual yield. This result may be attributed to a physical barrier effect, resulting from the fact that SiO_2 would prevent the transport of decomposition products in the polymer nanocomposites. Similar observations have been reported that the thermal stability of elastomer/SiO_2 nanocomposites was improved by a physical barrier effect, enhanced by reassembling of the silicate layer.[15] Therefore, the TGA results demonstrate that the incorporation of a small quantity of SiO_2 can significantly improve the thermal stability of the PLA-*g*-AA/SiO_2 nanocomposites.

Mechanical properties of hybrids

The stress–strain curves of the PLA-*g*-AA/SiO_2 nanocomposites with different SiO_2 content are shown in Figure 10. In all cases, the curves are linear at low strain followed by plastic deformation in the region of 2% strain. At higher strains the films yield up to a breaking strain 4% for the PLA-*g*-AA. This breaking strain tends to decrease with increasing SiO_2 content and occurs at $\sim$ 2.0% for the 16 wt % composite followed by a stiffing of the material. This behavior may be due to strain induced crystallization of the polymer resulting in material hardening.[22] Similar to the effect of SiO_2 content on the thermal property, it can be seen from Figure 10 that the tensile strength of PLA-*g*-AA/SiO_2 hybrids increases rapidly with the increasing of SiO_2 content from 0 to 10 wt % and then the tensile strength improves slightly. The positive effect on tensile strength may be due to the stiffness of the SiO_2 layers contributing to the presence of immobilized or partially immobilized polymer phases,[16] high aspect ratio and surface area of SiO_2, and the nanoscale dispersion of SiO_2 layers in the polymer matrix. It is also possible that SiO_2 layer orientation as well as molecular orientation contribute to the observed reinforcement effect. The slight decrease in tensile strength for the SiO_2 content beyond 10 wt % could be attributed to the inevitable aggregation of the excess SiO_2.

Figure 11 shows the variations of tensile strength at break with the WF content for PLA/WF, PLA-*g*-AA/WF, and PLA-*g*-AA/SiO_2/WF blends. It can be seen that the tensile strength of pure PLA is decreased when it is grafted with AA. The solid circles in Figure 11 illustrate that the tensile strength at break of PLA/WF blends decrease continuously and markedly from 53.5 to 18.8 MPa as the WF content is increased form 0 to 50 wt %. The deterioration in mechanical properties of PLA/WF blends may be due to the larger WF phase size (Table III) and the wide difference in character between the hydrophobic PLA and the hydrophilic. For PLA-*g*-AA/WF blends, as shown by the hollow circles in Figure 11, a quite different behavior of the tensile strength at break can be found, namely, the tensile strength at break increases with an increasing of WF content, although PLA-*g*-AA has a lower value of the tensile strength than that of the pure PLA. It is also found that the PLA-*g*-AA/WF blends not only give larger values of tensile strength than those of the PLA/WF blends but also provide stable values of the tensile strength when the WF content is beyond 10 wt %. A contribution to this result may

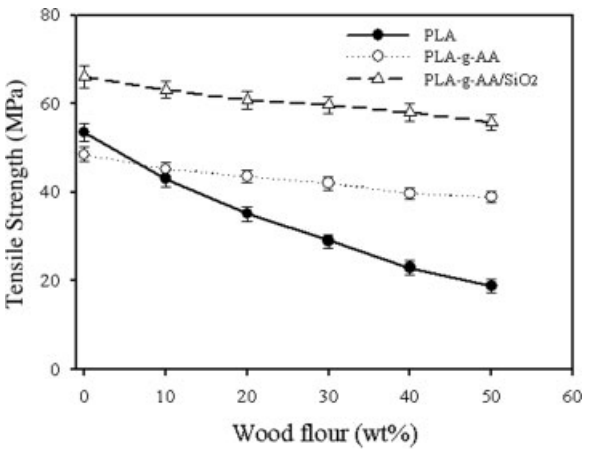

Figure 11 Tensile strength at break versus starch content for PLA, PLA-*g*-AA and PLA-*g*-AA/SiO_2 blends.

be due to the better dispersion and smaller phase size of WF in the PLA-*g*-AA matrix (Table III). This better dispersion may arise from the formation of branched and crosslinked macromolecules, since this PLA-*g*-AA copolymer has carboxylic acid groups to react with the hydroxyls of WF. These macromolecules have higher tensile strength, as compared with the linear ones. For PLA-*g*-AA/SiO_2/WF blends (the hollow triangles in Fig. 11), as compared with PLA/WF and PLA-*g*-AA/WF blends, much enhancement on the values of the tensile strength at break can be observed. The much better mechanical properties provided by the PLA-*g*-AA/SiO_2/WF blends may be coming from the much smaller WF phase size (Table III), the nanoscale dispersion of silicate layers in the polymer matrix, and the formation of the Si—O—C bond from the reaction between the PLA-*g*-AA and the silicate phase of SiO_2.

CONCLUSIONS

In this article, biodegradable organic–inorganic hybrids were prepared by an *in situ* sol–gel process and the melt blending method. FTIR spectra verified that the AA had been grafted onto the PLA copolymer and the Si—O—C bonds were formed in the PLA-*g*-AA/SiO_2 hybrid. The newly formed chemical bonds were produced through the dehydration of carboxylic acid groups in the PLA-*g*-AA with residual silanol groups in the silicate network. Additionally, as a result of the ^{29}Si solid-state NMR analysis, it was found that Si atom coordination around SiO_4 units is predominantly Q_3 and Q_4. This result was in agreement with structural interpretation of the FTIR spectra. TGA tests showed that the PLA-*g*-AA/SiO_2 hybrids produced higher values of IDT than the equivalent PLA/SiO_2. For example, an increment of 30°C can be observed for the addition of 10 wt % SiO_2 due to the formation of Si—O—C bond, and the nanoscale dispersion of silicate layers in the polymer matrix. Meanwhile, maximum tensile strength and glass transition temperature values occurred at about 10 wt % SiO_2 for PLA-*g*-AA/SiO_2 hybrids. Above 10 wt % SiO_2, excess silica particles may cause separation between the organic and inorganic phases, so reducing the compatibility between the silica network and PLA-*g*-AA. As compared with the pure polymer, PLA/SiO_2 showed only a small change in T_g, consistent with the relatively poor bonding between the organic and inorganic phase. However, with the PLA-*g*-AA chains chemically end linked into the inorganic network, the shifts in T_g were much larger, due to the interfacial forces of PLA-*g*-AA/SiO_2 associated with the Si—O—C and hetero-associated hydrogen bonds. The PLA/SiO_2, on the other hand, only has weaker hydrogen bonds. The PLA-*g*-AA/SiO_2 hybrid is a significant improvement over PLA/SiO_2 as far as its thermal and mechanical properties are concerned, not least the enhancement in T_g. Such properties could be useful in a variety of high-temperature applications. To improve the biodegradable property of the PLA/SiO_2 hybrids, the WF is chosen as the organic filler and the result shows that PLA-*g*-AA/SiO_2/WF hybrids could markedly improve the thermal and mechanical properties of PLA/WF and PLA-*g*-AA/WF hybrids since the nanoscale dispersion of silica layers, the smallest WF phase size, and the primary valence forces can be obtained in the PLA-*g*-AA/SiO_2/WF hybrids. Finally, the biodegradable PLA-*g*-AA/SiO_2/WF nanocomposites produced from our laboratory can provide a plateau tensile strength at break when the WF content is up to 50 wt%.

References

1. Arvanitoyannis, I.; Nakayama, A.; Kawasaki, N.; Yamamoto, N. Polymer 1995, 36, 2947.
2. Gupta, B.; Revagade, N.; Hilborn, J. Prog Polym Sci 2007, 32, 455.
3. Reeve, M. S.; McCarthy, S. P.; Downey, M. J.; Gross, R. A. Macromolecules 1994, 27, 825.
4. Arvanitoyannis, I. J Macromol Sci-Rev Macromol Chem Phys 1999, C39, 205.
5. Arvanitoyannis, I.; Psomiadou, E.; Yamamoto, N.; Blanshard, J. M. V. Polymer 1995, 36, 493.
6. Rizvi, G. M.; Park, C. B.; Lin, W. S.; Guo, G.; Pop-Iliev, R. Polym Eng Sci 2003, 43, 1347.
7. Lin, Q.; Zhou, X.; Dai, G. J Appl Polym Sci 2002, 85, 2824.
8. Ichazo, M. N.; Hernández, M.; Albano, C.; González, J. Macromol Symp 2006, 239, 192.
9. Zhang, M. Q.; Rong, M. Z.; Lu, X. Compos Sci Technol 2005, 15/16, 2514.
10. Ozaki, S. K.; Monteiro, M. B. B.; Yano, H.; Imamura, Y.; Souza, M. F. Polymer Degrad Stab 2005, 87, 293.
11. Yang, H.-S.; Wolcott, M. P.; Kim, S.; Kim, H.-S.; Kim H.-J. Polym Test 2006, 25, 668.
12. Thomas, J. K. Chem Rev 2005, 105, 1683.
13. Sykora, M.; Meyer, T. J. Chem Mater 1999, 11, 1186.
14. Perez-Bueno, J. J.; Vasquez-Garcia, S. R.; Garcia-Gonzalez, L.; Luna-Barcenas, G.; Gonzalez-Hernandez, J. J Phys Chem B 2002, 106, 1556.
15. Wu, C. S.; Liao, H. T. J Polym Sci Part B: Polym Phys 2003, 41, 351.
16. Wu, C. S. J Polym Sci Part A: Polym Chem 2005, 43, 1690.
17. Vaia, R. A.; Ishii, H.; Giannelis, E. P. Chem Mater 1993, 5, 1694.
18. Choi, H.; Sofranko, A. C.; Dionysiou, D. D. Adv Funct Mater 2006, 16, 1067.
19. Lee, C.-F.; Tsai, H.-H.; Wang, L.-Y.; Chen, C.-F.; Chiu, W.-Y. J Polym Sci Part A: Polym Chem 2005, 43, 342.
20. Inoue, S.-I.; Morita, K.; Asai, K.; Okamoto, H. J Appl Polym Sci 2004, 92, 2211.
21. Mark, J. E. Polym Eng Sci 1996, 36, 2905.
22. Schubert, U. Adv Eng Mater 2004, 6, 173.
23. Tong, X.; Tang, T.; Zhang, Q.; Feng, Z.; Huang, B. J Appl Polym Sci 2002, 83, 446.
24. Wu, C. S. Macromol Biosci 2005, 5, 352.

25. Young, S. K.; Jarrett, W. L.; Mauritz, K. A. Polym Eng Sci 2001, 41, 1529.
26. Wu, C. S.; Liao, H. T. Polymer 2005, 46, 10017.
27. Ma, X.; Yu, J.; Wang, N. J Polym Sci Part B: Polymer Phys 2006, 44, 94.
28. Gonsalves, K. E.; Jin, S.; Baraton, M.-I. Biomaterial 1998, 19, 1501.
29. Wu, C. S.; Liao, H. T. J Appl Polym Sci 2003, 88, 966.
30. Shao, P. L.; Mauritz, K. A.; Moore, R. B. J Polym Sci Part B: Polymer Phys 1996, 34, 873.
31. Wu, C. S.; Liao, H.T. Design Monomers Polym 2003, 6, 1.
32. Wu, K. H.; Chang, T. C.; Yang, J. C.; Chen, H. B. J Appl Polym Sci 2001, 79, 965.
33. Siudak, D. A.; Start, P. R.; Mauritz, K. A. J Appl Polym Sci 2000, 77, 2832.
34. Liao, H. T.; Wu, C. S. Macromol Mater Eng 2005, 290, 695.
35. Tsuji, H.; Fukui, I.; Daimon, H.; Fujie, K. Polym Degrad Stab 2003, 81, 501.
36. Siudak, F.; Nakane, K.; Piao, J. S. J Mater Sci 1996, 31, 1335.
37. Huang, Z. H.; Qju, K. Y. Polymer 1997, 38, 521.
38. Ji, X.-L.; Jiang, S.-C.; Qiu, X.-P.; Dong, D.-W.; Yu, D.-H.; Jiang, B.-Z. J Appl Polym Sci 2003, 88, 3168.